A Recurrent Mosaic Mutation in *SMO*, Encoding the Hedgehog Signal Transducer Smoothened, Is the Major Cause of Curry-Jones Syndrome

Stephen R.F. Twigg,[1] Robert B. Hufnagel,[2] Kerry A. Miller,[1] Yan Zhou,[1] Simon J. McGowan,[3] John Taylor,[4,5] Jude Craft,[4] Jenny C. Taylor,[4,6] Stephanie L. Santoro,[2] Taosheng Huang,[2] Robert J. Hopkin,[2] Angela F. Brady,[7] Jill Clayton-Smith,[8] Carol L. Clericuzio,[9] Dorothy K. Grange,[10] Leopold Groesser,[11] Christian Hafner,[11] Denise Horn,[12] I. Karen Temple,[13,14] William B. Dobyns,[15] Cynthia J. Curry,[16] Marilyn C. Jones,[17] and Andrew O.M. Wilkie[1,*]

Curry-Jones syndrome (CJS) is a multisystem disorder characterized by patchy skin lesions, polysyndactyly, diverse cerebral malformations, unicoronal craniosynostosis, iris colobomas, microphthalmia, and intestinal malrotation with myofibromas or hamartomas. Cerebellar medulloblastoma has been described in a single affected individual; in another, biopsy of skin lesions showed features of trichoblastoma. The combination of asymmetric clinical features, patchy skin manifestations, and neoplastic association previously led to the suggestion that this could be a mosaic condition, possibly involving hedgehog (Hh) signaling. Here, we show that CJS is caused by recurrent somatic mosaicism for a nonsynonymous variant in *SMO* (c.1234C>T [p.Leu412Phe]), encoding smoothened (SMO), a G-protein-coupled receptor that transduces Hh signaling. We identified eight mutation-positive individuals (two of whom had not been reported previously) with highly similar phenotypes and demonstrated varying amounts of the mutant allele in different tissues. We present detailed findings from brain MRI in three mutation-positive individuals. Somatic *SMO* mutations that result in constitutive activation have been described in several tumors, including medulloblastoma, ameloblastoma, and basal cell carcinoma. Strikingly, the most common of these mutations is the identical nonsynonymous variant encoding p.Leu412Phe. Furthermore, this substitution has been shown to activate SMO in the absence of Hh signaling, providing an explanation for tumor development in CJS. This raises therapeutic possibilities for using recently generated Hh-pathway inhibitors. In summary, our work uncovers the major genetic cause of CJS and illustrates strategies for gene discovery in the context of low-level tissue-specific somatic mosaicism.

The multiple-congenital-anomalies disorder Curry-Jones syndrome (MIM: 601707) was first presented (in abstract form) by Cynthia Curry and Marilyn Jones at the David W. Smith Workshop on Malformations and Morphogenesis in 1987. These authors described two unrelated individuals with the shared features of unilateral coronal craniosynostosis, cutaneous syndactyly, bilateral preaxial polydactyly of the feet, and unusual streaky skin lesions. Subsequently, the term Curry-Jones syndrome (CJS) was applied to this condition.[1,2]

The first formal publication on CJS was by Temple et al.[3] and included detailed clinical descriptions of the two original subjects and three further unrelated individuals. Four more simplex cases have since been added to the literature; each affected individual had abnormal skin patches and preaxial polydactyly of the feet.[4–6] Additional features found in most individuals have included ectopic hair growth, abnormalities of brain development, coloboma and/or microphthalmia, coronal suture synostosis, cutaneous syndactyly, and intestinal malrotation and/or obstruction (reviewed by Grange et al.[6]). Figures 1A–1D show the major craniofacial, limb, and dermatological features of CJS in a previously unreported individual (subject 8 in our series); MRI scans of three individuals (Figures 1E–1G) illustrate the diversity of cerebral malformations (described in more detail below). Mild intellectual disability has been present in some individuals. In a single individual, a desmoplastic medulloblastoma (World Health Organization grade IV) of the right cerebellum, found incidentally on a follow-up brain MRI scan at 17 months, was treated successfully by surgical resection, chemotherapy, and radiotherapy.[6] In two individuals,

[1]Clinical Genetics Group, Weatherall Institute of Molecular Medicine, John Radcliffe Hospital, University of Oxford, Oxford OX3 9DS, UK; [2]Division of Human Genetics, Department of Pediatrics, Cincinnati Children's Hospital Medical Center and University of Cincinnati College of Medicine, MLC 4006, 3333 Burnet Avenue, Cincinnati, OH 45229, USA; [3]Computational Biology Research Group, Weatherall Institute of Molecular Medicine, John Radcliffe Hospital, University of Oxford, Oxford OX3 9DS, UK; [4]Wellcome Trust Centre for Human Genetics, Roosevelt Drive, University of Oxford, Oxford OX3 7BN, UK; [5]Genetics Laboratories, Oxford University Hospitals NHS Foundation Trust, Churchill Hospital, Oxford OX3 7LE, UK; [6]Oxford Biomedical Research Centre, National Institute for Health Research, Oxford OX3 7BN, UK; [7]North West Thames Regional Genetics Service, Kennedy-Galton Centre, Northwick Park Hospital, Harrow HA1 3UJ, UK; [8]Manchester Centre for Genomic Medicine, St. Mary's Hospital, University of Manchester, Manchester M13 9WL, UK; [9]Division of Genetics/Dysmorphology, Department of Pediatrics, University of New Mexico, Albuquerque, NM 87131, USA; [10]Department of Pediatrics, Division of Genetics and Genomic Medicine, Washington University School of Medicine, St. Louis, MO 63110, USA; [11]Department of Dermatology, University of Regensburg, 93053 Regensburg, Germany; [12]Institute for Medical Genetics and Human Genetics, Charité Universitätsmedizin Berlin, 13353 Berlin, Germany; [13]Human Development and Health, Faculty of Medicine, University of Southampton, Southampton SO17 1BJ, UK; [14]Wessex Clinical Genetics Service, Princess Anne Hospital, University Hospital Southampton NHS Foundation Trust, Southampton SO16 6YD, UK; [15]Center for Integrative Brain Research, Seattle Children's Hospital, Seattle, WA 98105, USA; [16]Genetic Medicine, University of California, San Francisco, Fresno, CA 93701, USA; [17]Department of Pediatrics, University of California, San Diego, and Rady Children's Hospital, San Diego, CA 92123, USA
*Correspondence: andrew.wilkie@imm.ox.ac.uk
http://dx.doi.org/10.1016/j.ajhg.2016.04.007.

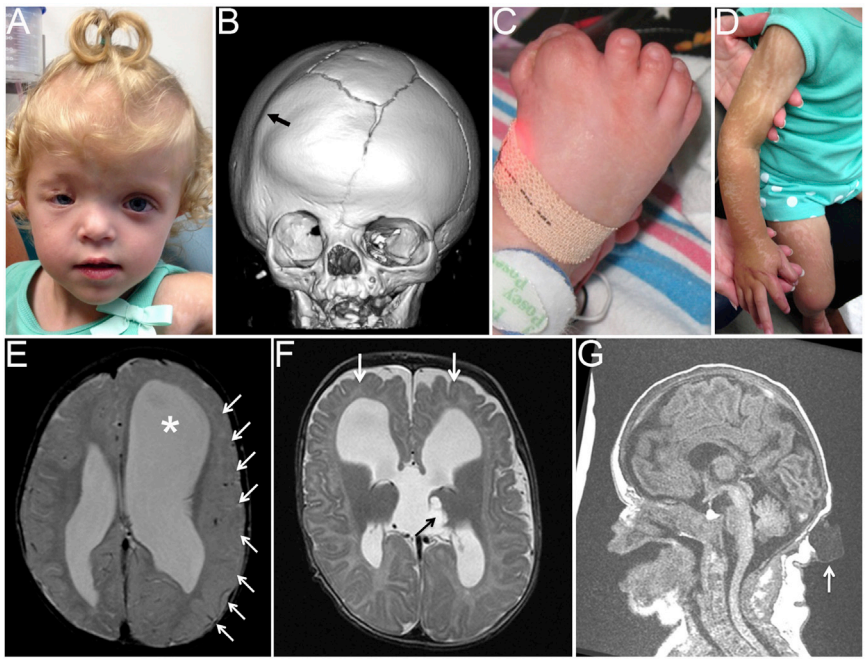

Figure 1. Clinical and Radiological Features and Brain Imaging of Individuals with CJS Caused by *SMO* Mutations
(A–D) Subject 8 at 2 years of age. (A) Facial features show asymmetry, frontal bossing, and scarring of the right eyelid. (B) Computed-tomographic head scan at 7 months of age shows right coronal synostosis (arrow), a bifurcated sagittal suture, and an anterior fontanellar bone. (C) The right foot is medially deviated with a duplicated hallux and partial cutaneous syndactyly of digits 1–3. (D) The skin has linear streaks of hypopigmentation with atrophy; this was not visible at birth but had developed by the age of 6 months.
(E–G) Brain MRI. (E) At 1 year, 5 months old, subject 5 shows left-sided hemimegalencephaly with extensive cortical malformation (arrows) and ventriculomegaly (asterisk). (F) At 3 months old, subject 6 shows subtle abnormalities of the gyri and cortex (white arrows); a cyst in the left thalamus (black arrow) connects with a third-ventricle midline cyst. (G) At 1 day old, subject 8 shows a thin corpus callosum, a mildly hypoplastic cerebellum, and an occipital cystic lesion pathologically confirmed to represent a lymphangiomatous malformation (white arrow).

biopsies of active skin lesions were reported to show features of either trichoblastoma[6] or nevus sebaceus.[3] In addition, odontogenic keratocysts have been found in one individual, and lesions in the bowel, identified histologically as hamartomas or myofibromas, were reported in three instances.[3,6]

The etiology of CJS was previously unknown, but three clinical observations are relevant to hypotheses for causation. First, the nine previously reported individuals comprised seven males and two females with similar disease severity, making an X-linked mutation unlikely. Second, the sporadic origin of all individuals in association with patchy skin lesions and asymmetric cranial findings led Temple et al.[3] to propose an underlying mosaic mutation; however, Grange et al.[6] favored a germline constitutional mutation in view of the consistent presentation and bilaterality of some of the other features. Third, the occurrence of medulloblastoma in basal cell nevus syndrome (BCNS [MIM: 109400])—caused by mutations in *PTCH1* (MIM: 601309), which encodes the hedgehog (Hh) receptor—as well as the overlapping cranial and limb abnormalities found in disorders caused by mutations in *GLI3* (MIM: 165240), a downstream effector of the Hh pathway, led Grange et al.[6] to propose that perturbation of Hh signaling could underlie CJS. However, sequencing of *PTCH1* and *GLI3* in DNA obtained from the blood of two individuals with CJS was normal.[6] The objective of the present work was to identify the causative mutation(s) underlying CJS through whole-exome sequencing (WES) by initially using an overlap strategy in four individuals to pinpoint disease-causing variants in the same gene.

The study was approved by Oxfordshire Research Ethics Committee B (reference C02.143) and the Riverside Research Ethics Committee (reference 09/H0706/20). Participants or their parents provided informed, written consent for genetic studies. Four of five samples initially chosen for analysis were from CJS-affected individuals reported by Temple et al.;[3] these comprised both eyelid tissue (sample 1-2, collected during an operation to repair a malformed upper eyelid with ectopic hairs) and fibroblasts from an affected skin biopsy (sample 1-4) from subject 1 (the individual originally described by Jones) and fibroblasts from affected skin of subjects 2 (sample 2-3) and 3 (sample 3-2), the latter of whom was the individual originally described by Curry. All fibroblast lines were analyzed between three and five passages. An additional fifth sample (4-1) was from the blood of subject 4, an unpublished individual with features overlapping CJS. The clinical features of these four individuals are summarized in Table 1.

After DNA extraction, we performed WES by using the SeqCap EZ Human Exome Library v.2.0 (NimbleGen) on a HiSeq 2000 (Illumina). Paired-end reads (100 bp) were mapped to hs37d5 with Stampy v.1.0.22,[7] and after removal of artifacts, the average coverage was >30× over 82% of the exome. We used Platypus[8] to call variants, and assuming that CJS is caused by very rare autosomally located variant(s), we prioritized the data by excluding common variants present in either our in-house database of solved cases or the NHLBI Exome Sequencing Project (ESP) Exome Variant Server (later revised to the Exome Aggregation Consortium [ExAC] Browser for reanalysis). We compared across CJS individuals for hits in the same gene. This analysis did not yield any genes with rare coding

Table 1. Clinical Features of Subjects Diagnosed with CJS

Subject	Gender	Craniosynostosis	Brain	Developmental Attainment	Eyes	Skin
1 (*SMO*$^+$)	F	RC	possible cyst in trigone of right ventricle	normal	R amblyopia; skin overgrowth	waxy, streaky lesions; nevus sebaceus
2 (*SMO*$^+$)	M	LC	ACC; R HMEG; R VMEG	mild delay	normal	raised, linear white streaks; normal biopsy
3 (*SMO*$^+$)	M	LC	partial ACC; asymmetric dilated ventricles	mild ID; IQ < 70	L and R microphthalmia; R iris coloboma	raised, scar-like pale lesions; non-specific biopsy
4	M	bicoronal	dilated ventricles; choroid plexus cyst	mild delay	congenital glaucoma; secondary cataract	pigmentary anomalies in Blashko's lines, most notable on limbs
5 (*SMO*$^+$)	M	none	mild ACC; L HMEG; R VMEG and PMG; occipital meningocele; Chiari I malformation	mild to moderate developmental delay	L mild colobomatous microphthalmia with unusually shaped pupil	raised, linear streaks (L arm and leg, chin, and a few other areas)
6 (*SMO*$^+$)	M	none	partial ACC; MEG; VMEG; Chiari I malformation	mild delay (1–2 years behind academically)	L and R iris colobomas	hypopigmented streaky lesions
7 (*SMO*$^+$)	M	none	normal	normal	normal	white, patchy skin behind knees
8 (*SMO*$^+$)	F	RC	partial ACC; moderate cerebral asymmetry consistent with L HMEG; PMG	mild delay	normal; dysmorphic R eyelid	linear areas of hypopigmented skin atrophy (extremities and trunk)
9	F	none	ACC; dilated ventricles; macrocephaly	psychomotor delay	bilateral colobomas of iris, retina, and choroid; strabismus; nystagmus	hypopigmented patch on trunk
10 (*SMO*$^+$)	F	LC	ACC; abnormal cortical dysplasia of R perirolandic region	psychomotor delay	corneal clouding; eyelid irregularity and ectopic hairs	mostly R-sided hypo- and hyperpigmented swirling skin lesions; increased hair in hyperpigmented areas

Abbreviations are as follows: F, female; M, male; LC, left coronal; RC, right coronal; R, right; L, left; ACC, agenesis of the corpus callosum; MEG, megalencephaly; HMEG, hemimegalencephaly; VMEG, ventriculomegaly; PMG, polymicrogyria; ID, intellectual disability; GI, gastrointestinal; H, hands; and F, feet.

(Table continued on next page)

Hair	GI Tract	Cutaneous Syndactyly	Polydactyly	Tumors	Other	Previously Reported?
ectopic patch of hair above R eye	GI bleeding; chronic constipation	L 1/2/3 (H); R 2/3 (H)	R trifid hallux	–	asymmetric face	case 4 in Temple et al.[3]
ectopic patch of hair near eyes	intestinal obstruction	L 2/3 (H), 3/4 (F); R 2/3/4 (H), 2/3 (F)	L and R broad thumbs, preaxial polydactyly (F)	myofibromas of large bowel	lip pits; seizures	case 1 in Temple et al.[3]
ectopic patch of hair above R eye	esophageal dysmotility	L and R 1/2/3/4 (H)	L and R bifid halluces	–	asymmetric face; fused central incisor; oligodontia; freckled areas on soles of feet; esophageal dysmotility	case 3 in Temple et al.[3]
chaotic hair patterning of lateral portions of eyebrows	diarrheal episodes	L and R 2/3/4 (F)	broad halluces	–	cleft palate	no
ectopic hair on cheek	malrotation; intestinal pseudo-obstruction; chronic constipation; subtotal colectomy for volvulus and obstipation	L 1/2/3/4 (H), 3/4 (F); R 2/3 (H), 3/4 (F)	L and R preaxial polydactyly (F); R thumb nubbin	desmoplastic medulloblastoma of cerebellum; odontogenic keratocysts; benign colonic polyps and smooth muscle hamartoma	large anterior fontanelle; lip pits	patient 2 in Grange et al.[6]
ectopic patch of hair near eyes	malrotation	L 1/2/3 (H), 1/2 (F); R 2/3 (H)	L and R preaxial polydactyly (H), preaxial polydactyly (F)	trichoblastoma; smooth muscle hamartomas of GI tract	mildly asymmetric face; lip pit	patient 1 in Grange et al.[6]
abnormal hair growth on shoulders and limbs	normal	R 1/2/3/4 (H)	L and R preaxial polydactyly (F); R: broad thumb	–	plagiocephaly	Thomas et al.[5]
–	malrotation; intermittent pseudo-obstruction; serosal nodules in the appendix, mesentery, and duodenum	L and R variable 1/2/3 (H and F)	L and R duplicated thumbs and halluces	scalp lymphangiomas: benign hamartomatous lesion with features of lymphangioma and nevus sebaceus; serosal hamartomas in duodenum, appendix, and mesentery	accessory bone at anterior fontanelle; wormian bones of L posterior skull; L leg longer than R; lumbar scoliosis	no
high frontal hairline	chronic constipation	L and R 3/4 (H)	L and R duplicated thumbs and halluces	lipomyelomeningocele	rudimentary sacral vertebrae	no
ectopic hairs; hirsutism	dysmotility; malrotation; multiple hamartomas of small intestine	R 1/2 (H)	L and R duplicated thumbs and halluces	multiple mesenteric hamartomas with smooth muscle bundles with inter-myenteric ganglia	grade 2 hydronephrosis	no

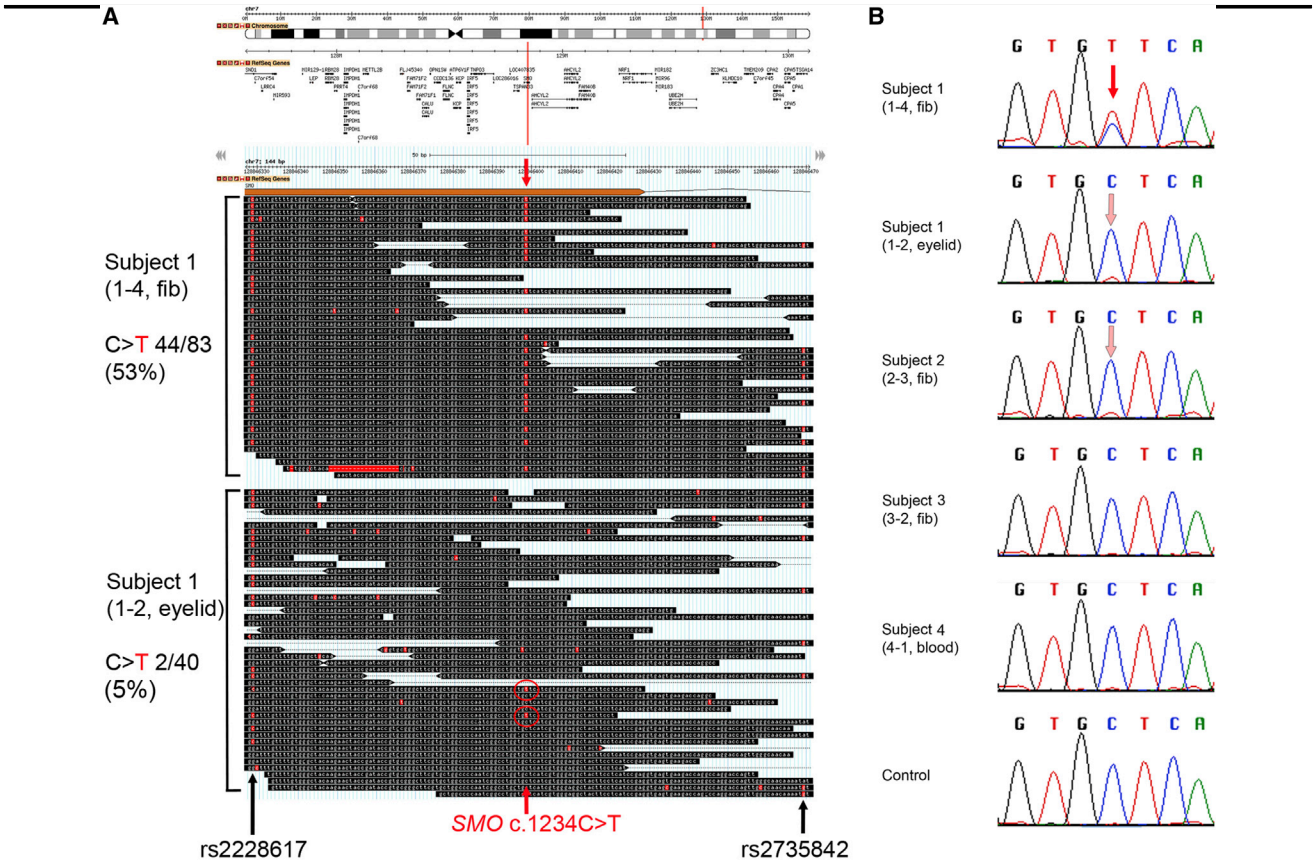

Figure 2. Identification of a Mosaic *SMO* c.1234C>T Mutation

(A) GBrowse[10] visualization of exome sequence data from two tissues of subject 1. The upper panel shows the location of *SMO* in chromosomal region 7q32.1, and the middle and lower panels display a 144 bp alignment of sequencing reads aligned to exon 6 and the following intron; bases that match the reference sequence are boxed in black, and variants are in red. The red arrows indicate the position of the c.1234C>T mutation (indicated by a "t" within a red box), which was present in 53% of reads in tissue 1-4 (middle panel; not all reads are shown) but only in 5% of reads in tissue 1-2 (lower panel). Flanking heterozygous SNPs are indicated by black arrows.

(B) Dideoxy-sequence traces for the c.1234C>T mutation. (Top) In sample 1-4, the mutation appears to be present in the heterozygous state, and there is no evidence of dilution by non-mutant cells (red arrow). (Middle) In samples 1-2 and 2-3, a small proportion of the mutant c.1234T allele is suspected to be present on the basis of both the presence of a small T peak and the reduced relative height of the normal C peak (pink arrows; compare with the control at bottom). By contrast, the mutation does not appear to be present in samples 3-2 and 4-1.

variants shared by three or four individuals, and only three genes had rare coding variants shared by two individuals, but none were strong candidates (Table S1).

As an alternative approach, we compared the data from the two tissues separately sequenced from subject 1, given that mosaicism for a pathogenic variant could be detectable through differences in allele frequencies between datasets. Variants were ranked according to a somatic p value score generated by the software tool MiG,[9] which compares variant and reference read counts between two datasets (Figure S1). The top hit was a nonsynonymous substitution in *SMO* (MIM: 601500; GenBank: NM_005631.4): c.1234C>T (p.Leu412Phe), present in 44 of 83 sequence reads from fibroblast sample 1-4. Notably, this variant was not called in the exome data from eyelid sample 1-2, although a low level of the same variant (2 of 40 sequence reads) was apparent on manual examination of the reads (Figure 2A). The fortuitous presence of two heterozygous flanking SNPs (rs2228617 and rs2735842; dbSNP137) in this individual enabled the two *SMO* alleles to be easily distinguished. We noted that when sequence reads included both the c.1234 position and one of the flanking SNPs, the mutant c.1234T reads were always in *cis* with the variant allele of the SNP in both samples. However, for the eyelid sample 1-2, the converse was not true, supporting the conclusion that the c.1234C>T mutation was mosaic in this sample (see Figure 2). *SMO* encodes smoothened (SMO), a frizzled G-protein-coupled receptor that plays a key role in transducing Hh signaling. Hh binding relieves patched-mediated suppression of SMO to allow transduction of the signal, probably mediated by conformational changes within the 7-transmembrane bundle.[11] Hence, the variant matched all three criteria (autosomal, mosaic, and affecting Hh signaling) for the characteristics of a candidate CJS-associated gene on the basis of clinical deduction.[3,6] Adding further weight to the conclusion

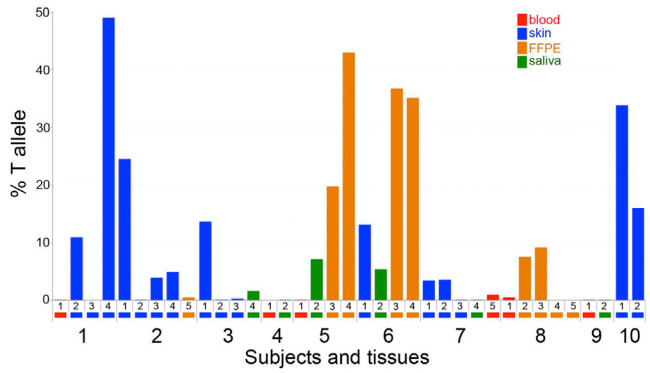

Figure 3. Quantification of Tissue Mosaicism for the *SMO* c.1234C>T Mutation

Plot of deep sequencing data shows the proportion of the mutant c.1234T allele in tissue samples collected from subjects 1–9. Similar tissue sources are grouped by color, indicated by a colored rectangle below the corresponding sample number. Individual tissue identifications along the horizontal axis correspond to the numbering listed in Table S2.

that this was the pathogenic variant, the Catalogue of Somatic Mutations in Cancer (COSMIC) revealed that *SMO* c.1234C>T is a known mutation hotspot in multiple tumor types (discussed further below). Dideoxy-sequencing of *SMO* exon 6 in sample 1-4 confirmed the presence of the C>T variant in an apparently heterozygous state, but the mutant peak was barely visible in sample 1-2 (Figure 2B).

In light of this finding, we scrutinized the exome sequence data for *SMO* from the other three CJS individuals in greater detail. The identical c.1234C>T variant was present in 2.7% (6 of 219) of reads from sample 2-3 (Figure S2) but was absent in the other two samples (0 of 57 reads from sample 3-2 and 0 of 179 reads from sample 4-1); no other suspicious *SMO* variant was detected in the exome sequences of subjects 3 or 4.

To gather further evidence that mosaic *SMO* mutations cause CJS, we collected and analyzed additional tissue samples from subjects 1–4 together with a further six individuals with CJS (subjects 5 and 6 reported by Grange et al.,[6] subject 7 reported by Thomas et al.,[5] and three unpublished individuals; clinical features are summarized in Table 1). Material from affected regions was prioritized and included archival formalin-fixed paraffin-embedded (FFPE) sections, such as those illustrated for affected skin and gut hamartoma in Grange et al.[6] (Table S2). We used the Ion Torrent PGM to perform deep sequencing of *SMO* exon 6 in a total of 37 different tissue samples from the ten CJS subjects (including the previously sequenced samples) and three control samples. Table S3 lists the primer sequences and conditions used for *SMO* (GenBank: NG_023340.1) amplification and sequencing. Deep sequencing of DNA from subject 1 confirmed a ~50% frequency for c.1234C>T in fibroblast sample 1-4 and showed that the variant was present at an 11% frequency in eyelid sample 1-2 (Figure 3 and Table S2). Surprisingly, we did not identify any mutant c.1234T alleles in the affected skin sample (1-3) from which the fibroblasts constituting sample 1-4 were derived, possibly indicating positive selection of mutant cells during growth in culture. In subject 2, the exome finding suggesting that the tested sample (2-3) was positive for an *SMO* mutation was validated, and c.1234C>T variant frequencies ranging from 4%–25% were detected in three of five samples, confirming mosaicism for the identical *SMO* mutation in this individual.

Deep sequencing of *SMO* in the samples used for exome sequencing (3-2 and 4-1) confirmed that the c.1234C>T mutation was essentially undetectable, given that the data were indistinguishable (by Fisher's exact test) from the control samples (Table S2). However, a new skin-biopsy sample from subject 3 was positive (14%), and a low level (1.6%) was detected in saliva. Furthermore, five of the six additional CJS individuals (subjects 5–8 and 10) were also mosaic for c.1234C>T (Figure 3 and Table S2). FFPE material from an occipital meningocele and cerebellar medulloblastoma were available from subject 5 (corresponding to patient 2 in Grange et al.[6]), and analysis showed relatively high levels of mosaicism for the c.1234T allele at 20% and 43%, respectively. Similarly, the abdominal smooth muscle tumor sections from subject 6 (patient 1 in Grange et al.;[6] samples 6-3 and 6-4) contained the c.1234T allele at 35%–37%. In subject 7, a mildly affected individual,[5] we detected c.1234T at 3%–4% in skin (sample 7-1, taken from a hairy area of the inner leg) and associated fibroblasts (7-2), as well as a femoral bone marrow sample (7-5, 1%). Finally, we identified the c.1234T variant in samples from two unpublished individuals, subjects 8 (Figures 1A–1D and 1G and Supplemental Note) and 10 (Table 1). FFPE samples from the colon (8-2) and cecum (8-3) collected from subject 8 during investigation of intestinal malrotation and mesenteric masses (which contained hamartomatous nodules consisting of disorganized bundles of mature smooth muscle intermixed with nerve fibers and ganglion cells) contained the c.1234T allele at levels of 8%–9%. In subject 10, an affected skin sample and derived fibroblasts contained c.1234T at 33% and 16%, respectively (Figure 3).

In total, we identified the identical *SMO* c.1234C>T mutation in tissues from eight unrelated CJS-affected individuals, including the two originally described by Curry and Jones. In all but one sample (1-4, in which the mutation was originally identified by exome sequencing), the c.1234T allele was present at a level substantially below 50%, indicating tissue mosaicism. Importantly for diagnosis, we had the greatest success in detecting the mutation in affected tissues obtained by invasive procedures. The mutation was not reliably detected in blood samples from three mutation-positive individuals (levels of c.1234T ranged from 0.03% to 0.5%, which we believe is below the threshold for clinical diagnosis [1%]; Figure 3 and Table S2). We had greater success with saliva samples (mean = 3.6% and range = 0.11%–7.1% in four mutation-positive individuals), but in every individual, a

different tissue sample showed a higher mutation level (Figure 3 and Table S2). This suggests that the optimum strategy for detecting mosaic mutations in CJS is to sample affected skin and tissue from internal organs if available. In subjects 4 and 9, from whom only blood and saliva samples were available, levels of the c.1234C>T mutation were 0.11% or lower. Although the results for some samples differed from those of control samples on formal statistical testing, they were deemed indeterminate for clinical purposes. Deep sequencing of the entire *SMO* coding region did not identify any alternative variants (data not shown). Analysis of tissue samples from affected regions would be required for determining whether these two individuals in fact carry the canonical mutation or have a distinct genetic basis for their phenotype.

The finding of widespread mosaicism in CJS suggests that it arises post-zygotically early during embryonic development. A somewhat later acquisition of the mutation is predicted to cause isolated pathology of individual organs, so we explored this possibility in the context of the skin. We performed deep sequencing of *SMO* in 14 isolated trichoblastoma samples and a single nevus sebaceus sample, given that analysis of skin biopsies from subjects 1 and 6 had previously demonstrated nevus sebaceus[3] and trichoblastoma,[6] respectively. Although we detected rare SNPs, we did not find potentially pathological variants (Table S4).

We sought to further define the neuroanatomical features of CJS by reviewing recent MRI scans of three mutation-positive individuals (subjects 5, 6, and 8). A diverse range of phenotypes were present in this small sample; prominent features are illustrated in Figures 1E–1G, and the complete phenotype is summarized in Table S5 and presented in Figure S3. Abnormal findings included hemimegalencephaly (HMEG) with cortical dysplasia, white-matter abnormalities and polymicrogyria, abnormalities of the corpus callosum, ventriculomegaly, occipital meningocele, and a Chiari type I malformation. Given the phenotypic overlap with isolated megalencephaly and/or HMEG and the previous observation of associated mutations in components of the PI3K-AKT pathway,[12–14] it would be of interest to test such mutation-negative brain samples for variants in *SMO*.

Although no constitutional mutations in *SMO* have previously been described, several hotspots of somatic mutation are evident in COSMIC, and it is striking that the most frequent of these is the identical c.1234C>T transition (note, this does not occur in the context of a CpG dinucleotide, so intrinsic hypermutability[15] is not predicted). Notably, the *SMO* c.1234C>T mutation has been identified in ameloblastoma,[16,17] medulloblastoma,[18,19] meningioma,[20,21] and basal cell carcinoma (BCC);[22,23] moreover, it has been reported as the oncogenic driver in some of these tumors.[16,23] The altered amino acid Leu412 locates to transmembrane helix 5 of SMO within one of three pivot regions that, by analogy with the β_2 adrenergic receptor,[24] are likely to have a key role in the conformational changes required for receptor activation. Supporting this, the presence of mutant p.Leu412Phe leads to constitutive activation in the absence of Hh ligand in *Smo*$^{-/-}$ mouse embryonic fibroblasts[16,22] and increased cell proliferation in ameloblast-lineage cells.[16]

Vertebrates have three Hh ligands, sonic hedgehog (SHH), desert hedgehog (DHH), and Indian hedgehog (IHH), which remove inhibition of SMO by binding to the receptor patched (encoded by *PTCH1* or *PTCH2* [MIM: 603673]). Downstream effectors of Hh signal transduction, notably the transcription factors GLI2 and GLI3, are normally tethered by SUFU (suppressor of fused homolog) at the base of the primary cilium, where they are proteolytically processed to repressor forms (GLI2-R and GLI3-R, respectively). SMO activation leads to KIF7-dependent translocation toward the tip of the primary cilium and to transport of full-length activated GLI proteins (GLI2-A and GLI3-A) into the nucleus, enabling transcriptional activation (reviewed by Briscoe and Therond,[25] McCabe and Leahy,[26] and Arensdorf et al.[27]). Activation of the PI3K-AKT-mTOR and/or PKA pathways can independently lead to GLI activation, indicating the potential for significant cross-talk with the Hh pathway.[28] Constitutional mutations that mimic the consequences of Hh signal activation include loss-of-function mutations in negative regulators acting at multiple stages of the Hh pathway, such as *RAB23* (associated with Carpenter syndrome [MIM: 606144]),[29] *PTCH1*[30–32] and *SUFU*[33,34] (associated with BCNS), *KIF7* (associated with acrocallosal syndrome),[35] and *GLI3* (associated with Greig cephalopolysyndactyly).[36,37] In addition, regulatory mutations in *IHH* (MIM: 600726) cause Philadelphia craniosynostosis.[38] Reflecting the net consequence of excessive Hh signal transduction, several clinical features of CJS overlap those of the above disorders, as previously noted.[6] These include craniosynostosis[39] in both Carpenter and Philadelphia craniosynostosis syndromes, preaxial polydactyly in Greig and Carpenter syndromes,[40] cerebral malformations in acrocallosal syndrome,[35] and odontogenic keratocysts and skin involvement in BCNS.[41] We also note overlap between the cerebral features and mosaic activation of components of the PI3K-AKT-mTOR pathway, such as in Proteus syndrome (MIM: 164730), fibroadipose hyperplasia and CLOVES syndrome (MIM: 612918), and HMEG (reviewed in Keppler-Noreuil et al.,[12] Hevner,[13] and Jansen et al.[14]). To our knowledge, abnormalities of the bowel have not previously been highlighted as a frequent feature of disorders associated with activation of Hh signaling, but they appear to be common in CJS (e.g., malrotation and myofibromas or hamartomas). These bowel abnormalities are consistent with the documented role of murine SHH and IHH, produced by the endodermal epithelium, as primary factors in the patterning and organogenesis of the gut,[42] where Hh signaling from the endoderm controls growth of the adjacent mesenchyme.[43] Mouse embryos in which *Smo* is deleted from the gut mesenchyme have severely reduced proliferation and differentiation of the

intestinal mesenchyme and a reduced number of smooth muscle cells and enteric neurons.[44]

Given the observed association between CJS and neoplastic diseases (trichoblastoma and cerebellar medulloblastoma), a particularly important consequence of identifying the activating p.Leu412Phe substitution in SMO concerns the potential pharmacotherapeutic implications for management of affected individuals. Recently, there has been considerable interest in developing SMO inhibitors to reduce activation of the Hh pathway (reviewed by Arensdorf et al.[27]). For example, vismodegib is a clinically approved SMO inhibitor that contacts the extracellular domain and ligand-binding pocket. Interestingly, in a recent report of a subject with segmental BCNS associated with the identical SMO p.Leu412Phe substitution,[45] treatment with vismodegib for 4 months led to cessation of the appearance of new lesions and shrinkage of some existing BCCs. However, other reports have suggested that the p.Leu412Phe substitution confers resistance to vismodegib, supporting a role for Leu412 in autoinhibition and/or structural stability.[22,23] This suggests that in CJS-associated tumors, the use of additional agents, such as arsenic trioxide or other more-specific GLI inhibitors or PI3K-AKT-mTOR inhibitors, that act at later stages of the Hh signal-transduction pathway should be explored,[33] and indeed there is evidence that this approach can be effective against p.Leu412Phe mutants.[16,22]

In summary, these data show that the major phenotypic features of CJS are attributable to excessive activation of Hh signaling owing to a specific c.1234C>T (p.Leu412Phe) somatic mutation. The finding that all eight mutation-positive individuals are mosaic might indicate that constitutional mutations are not compatible with life, as is true for several other sporadic autosomal disorders.[46] The mutation is likely to be associated with a spectrum of negative and positive selective consequences during organismal growth and homeostasis, depending on cell type, which most likely explains the apparent evolution of skin lesions and low mutation levels in blood (negative selection) and the predisposition to tumorigenesis (positive selection). The association between segmental BCNS and SMO p.Leu412Phe in a recent report[45] is compatible with a later occurrence of the somatic mutation during development than in subjects with the classical CJS phenotype.

Supplemental Data

Supplemental Data include a Supplemental Note, three figures, and five tables and can be found with this article online at http://dx.doi.org/10.1016/j.ajhg.2016.04.007.

Acknowledgments

We are grateful to all the families for their participation in this study. We thank the staff at the high-throughput genomics facility at the Wellcome Trust Centre for Human Genetics (Oxford Genomics Centre) for exome sequencing and Sue Butler, John Frankland, and Tim Rostron for help with cell culture and DNA sequencing. This work was supported by the National Institute for Health Research (NIHR) Oxford Biomedical Research Centre Programme (J.C.T. and A.O.M.W.), the Medical Research Council through the Weatherall Institute of Molecular Medicine Strategic Alliance (G0902418 and MC_UU_12025), and the Wellcome Trust (project grant 093329 to A.O.M.W. and S.R.F.T. and Senior Investigator Award 102731 to A.O.M.W.). The views expressed in this publication are those of the authors and not necessarily those of the National Health Service, NIHR, or Department of Health.

Received: February 8, 2016
Accepted: April 13, 2016
Published: May 26, 2016

Web Resources

COSMIC, http://cancer.sanger.ac.uk/cosmic
dbSNP, http://www.ncbi.nlm.nih.gov/projects/SNP/
Exome Aggregation Consortium (ExAC) Browser, http://exac.broadinstitute.org/
Leiden Open Variation Database (LOVD), http://chromium.lovd.nl/LOVD2
MiG: Multi-Image Genome, https://mig.molbiol.ox.ac.uk/mig/
NHLBI Exome Sequencing Project (ESP) Exome Variant Server, http://evs.gs.washington.edu/EVS/
OMIM, http://www.omim.org/
RefSeq, http://www.ncbi.nlm.nih.gov/RefSeq

References

1. Cohen, M.M., Jr. (1988). Craniosynostosis update 1987. Am. J. Med. Genet. Suppl. *4*, 99–148.
2. Gorlin, R.J., Cohen, M.M., Jr., and Levin, L.S. (1990). Syndromes with craniosynostosis: general aspects and well-known syndromes. In Syndromes of the Head and Neck (Oxford University Press), pp. 519–539.
3. Temple, I.K., Eccles, D.M., Winter, R.M., Baraitser, M., Carr, S.B., Shortland, D., Jones, M.C., and Curry, C. (1995). Craniofacial abnormalities, agenesis of the corpus callosum, polysyndactyly and abnormal skin and gut development–the Curry Jones syndrome. Clin. Dysmorphol. *4*, 116–129.
4. Mingarelli, R., Mokini, V., Castriota Scanderbeg, A., and Dallapiccola, B. (1999). Brachycephalosyndactyly with ptosis, cataract, colobomas, and linear areas of skin depigmentation. Clin. Dysmorphol. *8*, 73–75.
5. Thomas, E.R., Wakeling, E.L., Goodman, F.R., Dickinson, J.C., Hall, C.M., and Brady, A.F. (2006). Mild case of Curry-Jones syndrome. Clin. Dysmorphol. *15*, 115–117.
6. Grange, D.K., Clericuzio, C.L., Bayliss, S.J., Berk, D.R., Heideman, R.L., Higginson, J.K., Julian, S., and Lind, A. (2008). Two new patients with Curry-Jones syndrome with trichoblastoma and medulloblastoma suggest an etiologic role of the sonic hedgehog-patched-GLI pathway. Am. J. Med. Genet. A. *146A*, 2589–2597.
7. Lunter, G., and Goodson, M. (2011). Stampy: a statistical algorithm for sensitive and fast mapping of Illumina sequence reads. Genome Res. *21*, 936–939.
8. Rimmer, A., Phan, H., Mathieson, I., Iqbal, Z., Twigg, S.R., Wilkie, A.O., McVean, G., and Lunter, G.; WGS500 Consortium (2014). Integrating mapping-, assembly- and haplotype-based approaches for calling variants in clinical sequencing applications. Nat. Genet. *46*, 912–918.

9. McGowan, S.J., Hughes, J.R., Han, Z.P., and Taylor, S. (2013). MIG: Multi-Image Genome viewer. Bioinformatics *29*, 2477–2478.
10. Stein, L.D., Mungall, C., Shu, S., Caudy, M., Mangone, M., Day, A., Nickerson, E., Stajich, J.E., Harris, T.W., Arva, A., and Lewis, S. (2002). The generic genome browser: a building block for a model organism system database. Genome Res. *12*, 1599–1610.
11. Wang, C., Wu, H., Katritch, V., Han, G.W., Huang, X.P., Liu, W., Siu, F.Y., Roth, B.L., Cherezov, V., and Stevens, R.C. (2013). Structure of the human smoothened receptor bound to an antitumour agent. Nature *497*, 338–343.
12. Keppler-Noreuil, K.M., Rios, J.J., Parker, V.E., Semple, R.K., Lindhurst, M.J., Sapp, J.C., Alomari, A., Ezaki, M., Dobyns, W., and Biesecker, L.G. (2015). *PIK3CA*-related overgrowth spectrum (PROS): diagnostic and testing eligibility criteria, differential diagnosis, and evaluation. Am. J. Med. Genet. A. *167A*, 287–295.
13. Hevner, R.F. (2015). Brain overgrowth in disorders of RTK-PI3K-AKT signaling: a mosaic of malformations. Semin. Perinatol. *39*, 36–43.
14. Jansen, L.A., Mirzaa, G.M., Ishak, G.E., O'Roak, B.J., Hiatt, J.B., Roden, W.H., Gunter, S.A., Christian, S.L., Collins, S., Adams, C., et al. (2015). PI3K/AKT pathway mutations cause a spectrum of brain malformations from megalencephaly to focal cortical dysplasia. Brain *138*, 1613–1628.
15. Rahbari, R., Wuster, A., Lindsay, S.J., Hardwick, R.J., Alexandrov, L.B., Al Turki, S., Dominiczak, A., Morris, A., Porteous, D., Smith, B., et al.; UK10K Consortium (2016). Timing, rates and spectra of human germline mutation. Nat. Genet. *48*, 126–133.
16. Sweeney, R.T., McClary, A.C., Myers, B.R., Biscocho, J., Neahring, L., Kwei, K.A., Qu, K., Gong, X., Ng, T., Jones, C.D., et al. (2014). Identification of recurrent *SMO* and *BRAF* mutations in ameloblastomas. Nat. Genet. *46*, 722–725.
17. Brown, N.A., Rolland, D., McHugh, J.B., Weigelin, H.C., Zhao, L., Lim, M.S., Elenitoba-Johnson, K.S., and Betz, B.L. (2014). Activating *FGFR2-RAS-BRAF* mutations in ameloblastoma. Clin. Cancer Res. *20*, 5517–5526.
18. Jones, D.T., Jäger, N., Kool, M., Zichner, T., Hutter, B., Sultan, M., Cho, Y.J., Pugh, T.J., Hovestadt, V., Stütz, A.M., et al. (2012). Dissecting the genomic complexity underlying medulloblastoma. Nature *488*, 100–105.
19. Pugh, T.J., Weeraratne, S.D., Archer, T.C., Pomeranz Krummel, D.A., Auclair, D., Bochicchio, J., Carneiro, M.O., Carter, S.L., Cibulskis, K., Erlich, R.L., et al. (2012). Medulloblastoma exome sequencing uncovers subtype-specific somatic mutations. Nature *488*, 106–110.
20. Brastianos, P.K., Horowitz, P.M., Santagata, S., Jones, R.T., McKenna, A., Getz, G., Ligon, K.L., Palescandolo, E., Van Hummelen, P., Ducar, M.D., et al. (2013). Genomic sequencing of meningiomas identifies oncogenic *SMO* and *AKT1* mutations. Nat. Genet. *45*, 285–289.
21. Clark, V.E., Erson-Omay, E.Z., Serin, A., Yin, J., Cotney, J., Ozduman, K., Avşar, T., Li, J., Murray, P.B., Henegariu, O., et al. (2013). Genomic analysis of non-*NF2* meningiomas reveals mutations in *TRAF7*, *KLF4*, *AKT1*, and *SMO*. Science *339*, 1077–1080.
22. Atwood, S.X., Sarin, K.Y., Whitson, R.J., Li, J.R., Kim, G., Rezaee, M., Ally, M.S., Kim, J., Yao, C., Chang, A.L., et al. (2015). Smoothened variants explain the majority of drug resistance in basal cell carcinoma. Cancer Cell *27*, 342–353.
23. Sharpe, H.J., Pau, G., Dijkgraaf, G.J., Basset-Seguin, N., Modrusan, Z., Januario, T., Tsui, V., Durham, A.B., Dlugosz, A.A., Haverty, P.M., et al. (2015). Genomic analysis of smoothened inhibitor resistance in basal cell carcinoma. Cancer Cell *27*, 327–341.
24. Katritch, V., Cherezov, V., and Stevens, R.C. (2013). Structure-function of the G protein-coupled receptor superfamily. Annu. Rev. Pharmacol. Toxicol. *53*, 531–556.
25. Briscoe, J., and Thérond, P.P. (2013). The mechanisms of Hedgehog signalling and its roles in development and disease. Nat. Rev. Mol. Cell Biol. *14*, 416–429.
26. McCabe, J.M., and Leahy, D.J. (2015). Smoothened goes molecular: new pieces in the hedgehog signaling puzzle. J. Biol. Chem. *290*, 3500–3507.
27. Arensdorf, A.M., Marada, S., and Ogden, S.K. (2016). Smoothened regulation: a tale of two signals. Trends Pharmacol. Sci. *37*, 62–72.
28. Wang, Y., Ding, Q., Yen, C.J., Xia, W., Izzo, J.G., Lang, J.Y., Li, C.W., Hsu, J.L., Miller, S.A., Wang, X., et al. (2012). The crosstalk of mTOR/S6K1 and Hedgehog pathways. Cancer Cell *21*, 374–387.
29. Jenkins, D., Seelow, D., Jehee, F.S., Perlyn, C.A., Alonso, L.G., Bueno, D.F., Donnai, D., Josifova, D., Mathijssen, I.M., Morton, J.E., et al. (2007). *RAB23* mutations in Carpenter syndrome imply an unexpected role for hedgehog signaling in cranial-suture development and obesity. Am. J. Hum. Genet. *80*, 1162–1170.
30. Hahn, H., Wicking, C., Zaphiropoulous, P.G., Gailani, M.R., Shanley, S., Chidambaram, A., Vorechovsky, I., Holmberg, E., Unden, A.B., Gillies, S., et al. (1996). Mutations of the human homolog of Drosophila patched in the nevoid basal cell carcinoma syndrome. Cell *85*, 841–851.
31. Johnson, R.L., Rothman, A.L., Xie, J., Goodrich, L.V., Bare, J.W., Bonifas, J.M., Quinn, A.G., Myers, R.M., Cox, D.R., Epstein, E.H., Jr., and Scott, M.P. (1996). Human homolog of patched, a candidate gene for the basal cell nevus syndrome. Science *272*, 1668–1671.
32. Ming, J.E., Kaupas, M.E., Roessler, E., Brunner, H.G., Golabi, M., Tekin, M., Stratton, R.F., Sujansky, E., Bale, S.J., and Muenke, M. (2002). Mutations in PATCHED-1, the receptor for SONIC HEDGEHOG, are associated with holoprosencephaly. Hum. Genet. *110*, 297–301.
33. Kool, M., Jones, D.T., Jäger, N., Northcott, P.A., Pugh, T.J., Hovestadt, V., Piro, R.M., Esparza, L.A., Markant, S.L., Remke, M., et al.; ICGC PedBrain Tumor Project (2014). Genome sequencing of SHH medulloblastoma predicts genotype-related response to smoothened inhibition. Cancer Cell *25*, 393–405.
34. Smith, M.J., Beetz, C., Williams, S.G., Bhaskar, S.S., O'Sullivan, J., Anderson, B., Daly, S.B., Urquhart, J.E., Bholah, Z., Oudit, D., et al. (2014). Germline mutations in *SUFU* cause Gorlin syndrome-associated childhood medulloblastoma and redefine the risk associated with *PTCH1* mutations. J. Clin. Oncol. *32*, 4155–4161.
35. Putoux, A., Thomas, S., Coene, K.L., Davis, E.E., Alanay, Y., Ogur, G., Uz, E., Buzas, D., Gomes, C., Patrier, S., et al. (2011). *KIF7* mutations cause fetal hydrolethalus and acrocallosal syndromes. Nat. Genet. *43*, 601–606.
36. Vortkamp, A., Gessler, M., and Grzeschik, K.H. (1991). GLI3 zinc-finger gene interrupted by translocations in Greig syndrome families. Nature *352*, 539–540.
37. Johnston, J.J., Sapp, J.C., Turner, J.T., Amor, D., Aftimos, S., Aleck, K.A., Bocian, M., Bodurtha, J.N., Cox, G.F., Curry, C.J., et al. (2010). Molecular analysis expands the spectrum of

phenotypes associated with *GLI3* mutations. Hum. Mutat. *31*, 1142–1154.

38. Klopocki, E., Lohan, S., Brancati, F., Koll, R., Brehm, A., Seemann, P., Dathe, K., Stricker, S., Hecht, J., Bosse, K., et al. (2011). Copy-number variations involving the *IHH* locus are associated with syndactyly and craniosynostosis. Am. J. Hum. Genet. *88*, 70–75.
39. Twigg, S.R.F., and Wilkie, A.O.M. (2015). A genetic-pathophysiological framework for craniosynostosis. Am. J. Hum. Genet. *97*, 359–377.
40. Anderson, E., Peluso, S., Lettice, L.A., and Hill, R.E. (2012). Human limb abnormalities caused by disruption of hedgehog signaling. Trends Genet. *28*, 364–373.
41. Athar, M., Li, C., Kim, A.L., Spiegelman, V.S., and Bickers, D.R. (2014). Sonic hedgehog signaling in Basal cell nevus syndrome. Cancer Res. *74*, 4967–4975.
42. Ramalho-Santos, M., Melton, D.A., and McMahon, A.P. (2000). Hedgehog signals regulate multiple aspects of gastrointestinal development. Development *127*, 2763–2772.
43. Mao, J., Kim, B.M., Rajurkar, M., Shivdasani, R.A., and McMahon, A.P. (2010). Hedgehog signaling controls mesenchymal growth in the developing mammalian digestive tract. Development *137*, 1721–1729.
44. Huang, H., Cotton, J.L., Wang, Y., Rajurkar, M., Zhu, L.J., Lewis, B.C., and Mao, J. (2013). Specific requirement of Gli transcription factors in Hedgehog-mediated intestinal development. J. Biol. Chem. *288*, 17589–17596.
45. Khamaysi, Z., Bochner, R., Indelman, M., Magal, L., Avitan-Hersh, E., Sarig, O., Sprecher, E., and Bergman, R. (2016). Segmental Basal cell nevus syndrome caused by an activating mutation in Smoothened. Br. J. Dermatol. http://dx.doi.org/10.1111/bjd.14425.
46. Happle, R. (2016). The categories of cutaneous mosaicism: A proposed classification. Am. J. Med. Genet. A. *170*, 452–459.

The American Journal of Human Genetics, Volume *98*

Supplemental Data

A Recurrent Mosaic Mutation in *SMO*, Encoding the Hedgehog Signal Transducer Smoothened, Is the Major Cause of Curry-Jones Syndrome

Stephen R.F. Twigg, Robert B. Hufnagel, Kerry A. Miller, Yan Zhou, Simon J. McGowan, John Taylor, Jude Craft, Jenny C. Taylor, Stephanie L. Santoro, Taosheng Huang, Robert J. Hopkin, Angela F. Brady, Jill Clayton-Smith, Carol L. Clericuzio, Dorothy K. Grange, Leopold Groesser, Christian Hafner, Denise Horn, I. Karen Temple, William B. Dobyns, Cynthia J. Curry, Marilyn C. Jones, and Andrew O.M. Wilkie

Supplemental Note: Clinical report

Subject 8

This female child was assessed at the age of 2 years. She had been born at 36 weeks' gestation to a 29 year old G3P2 mother and a 28 year old father. Fetal MRI was performed at 29 weeks' gestation because of occipital cystic swellings observed on a previous ultrasound scan. The MRI demonstrated facial abnormalities, abnormal right calvarial shape and frontal lobe sulcation, consistent with craniosynostosis, unilateral right microcephaly, and focal polymicrogyria. Occipital scalp lymphangiomas and bowel malrotation were also noted. At birth, she was noted to have facial asymmetry and duplicated syndactylous thumbs and halluces with variable syndactyly of digits 1-3 in all extremities. Dysmorphic features included scalp lymphangiomas, frontal bossing, flat nasal bridge, midface retrusion, prominent chin, and large ears. Postnatal brain MRI confirmed the prenatal findings, with the addition of cavum septum pellucidum with intact corpus callosum. Head computed tomography (CT) revealed extensive right coronal craniosynostosis, accessory bone at the anterior fontanelle, wormian bones of the left posterior skull, enlarged right lateral ventricle, and prominent extra-axial spaces. The scalp lymphangiomas were excised shortly after birth, and histologically described as hamartomatous lesions with features of lymphangioma and nevus sebaceus.

Early feeding difficulties prompted further investigation and bowel malrotation was discovered, requiring band division (Ladd's procedure) and ileostomy, which was later reversed. Serosal nodules noted in the duodenum, appendix, and mesentery were pathologically characterized as hamartomatous with fibrovascular and neuromuscular components. Subsequently, she has had extensive malabsorption, diarrhea, and intermittent pseudo-obstruction. Vesicoureteral reflux from birth caused frequent urinary tract infections. Although not present at birth, by 6 months of age linear areas of pigmentary mosaicism were evident over the extremities and trunk, while sparing the face and scalp; based on the failure to tan normally, the affected skin appeared to be the hypopigmented and atrophic component. Around 1.5 years of age, she was noted to have significant leg length discrepancy, left greater than right, and lumbar scoliosis. Her development has progressed well despite her complex problems, and she is walking, speaking in two word sentences, has pincer grasp, and is socially engaged. Currently, her height, weight, and head circumference are within the normal range.

Genetic testing results, including karyotype, SNP-based microarray, chromosome breakage studies, sequencing and deletion/duplication testing of *RECQL4*, *TWIST*, *FGFR1*, and *FGFR2*, selective mutational analysis of *FGFR3*, and clinical whole exome sequencing from blood-derived DNA did not indicate disease-causing mutations accounting for her phenotype.

Figure S1. *SMO* is the top hit in an analysis of variant allele frequency differences in two samples from Subject 1.

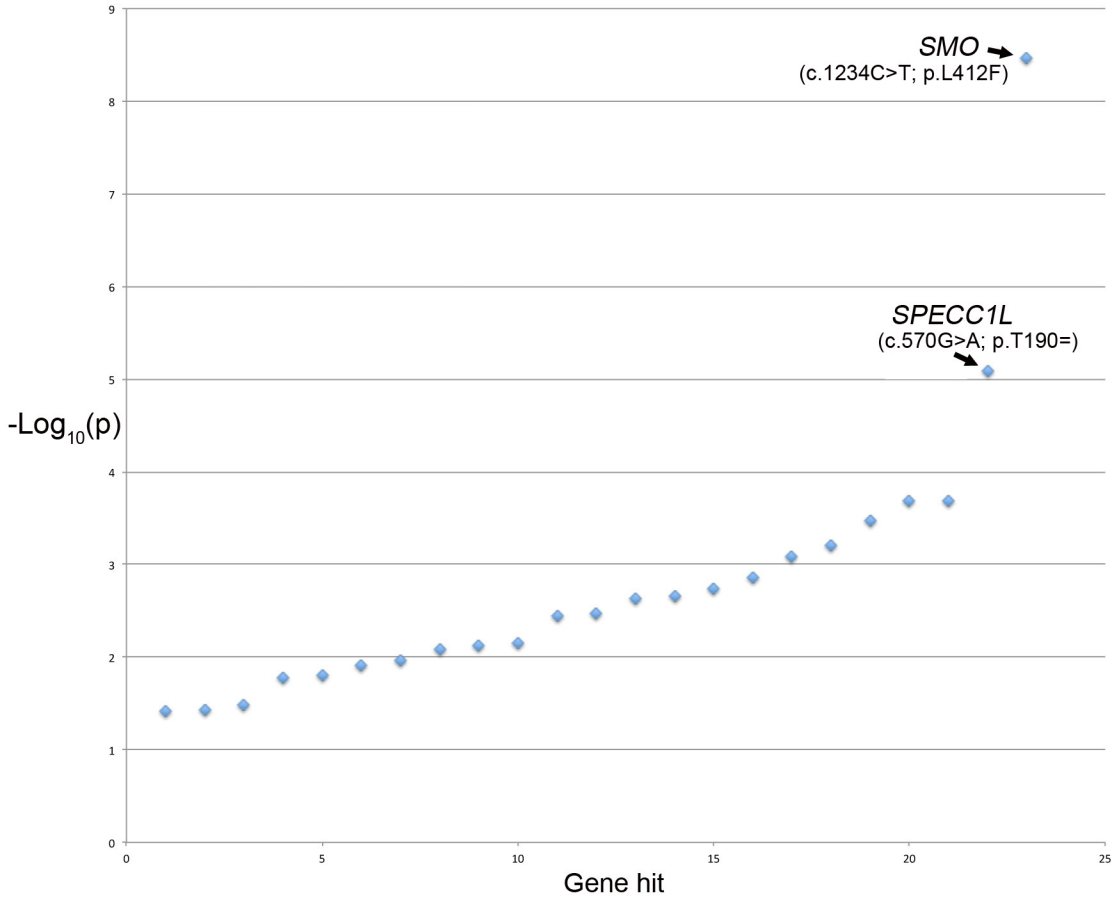

The exome data from Subject 1 (samples 1-2 and 1-4) was analysed using MiG (Multi-Image Genome viewer; McGowan et al., 2013). Only variants within exons and at positions with read depths greater than or equal to 20 were considered. A p-value threshold of 0.05 was used in the calling of somatic sites (threshold below which read count differences between two samples were deemed nominally significant). The variant frequency cutoff applied to the data was ≤15% in one tissue, and ≥30% in the other tissue, and vice versa. The 23 variant hits are shown plotted against $-\text{Log}_{10}(p)$.

Figure S2. Exome sequence of *SMO* exon 6 from Subject 2.

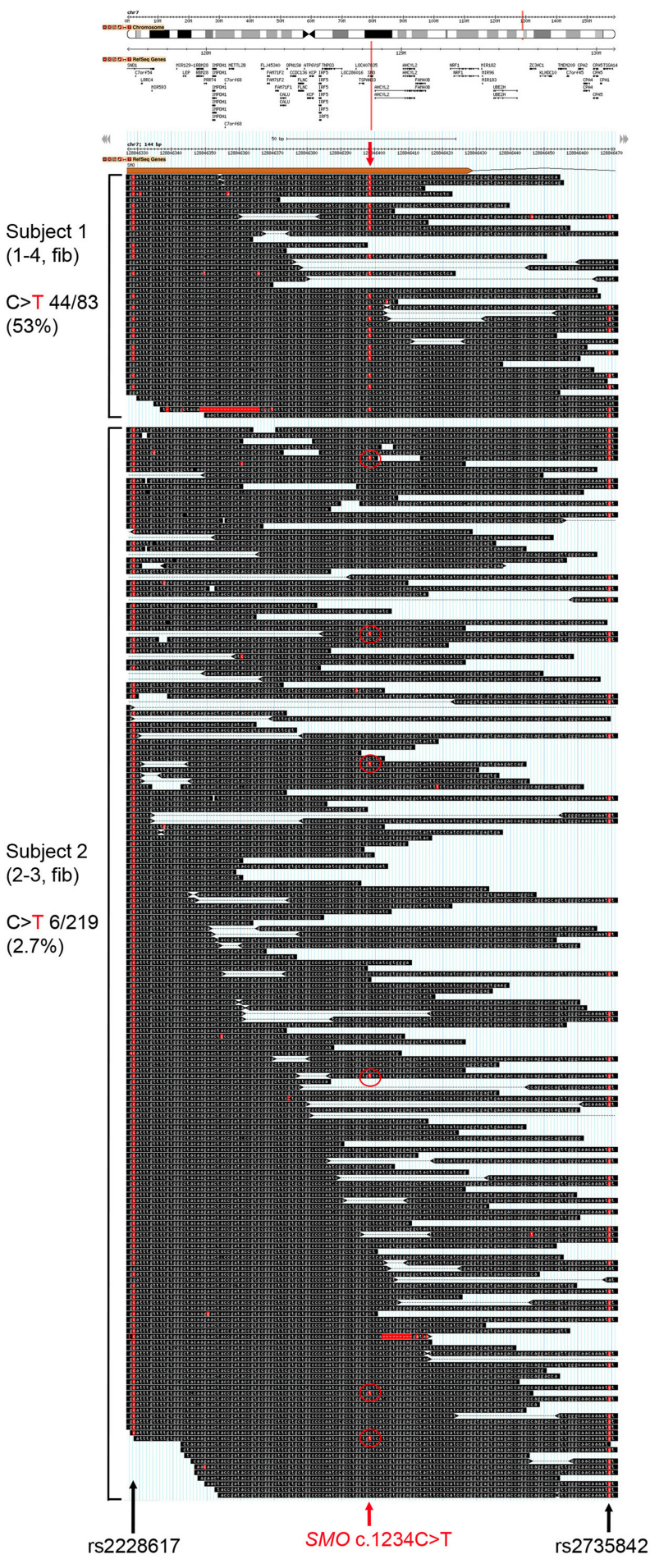

Exome sequencing reads, visualized in GBrowse, aligned to *SMO* exon 6 from Subject 1 (sample 1-4, not all reads are shown) shown above, and Subject 2 (sample 2-3), below. The red arrow indicates the 1234C>T mutation position. Mutant T reads in Subject 2 (6/219 reads) are circled for clarity and make up 2.7% of nucleotides at this position. The two flanking SNPs, rs2228617 upstream and rs2735842 downstream, are indicated by black arrows, and are both homozygous for the variant allele in Subject 2. The uppermost panel shows the position of *SMO*, and nearby genes, on chromosome 7q32.1.

Figure S3. Magnetic resonance imaging of brains of Subjects 5, 6 and 8.

Subject 5

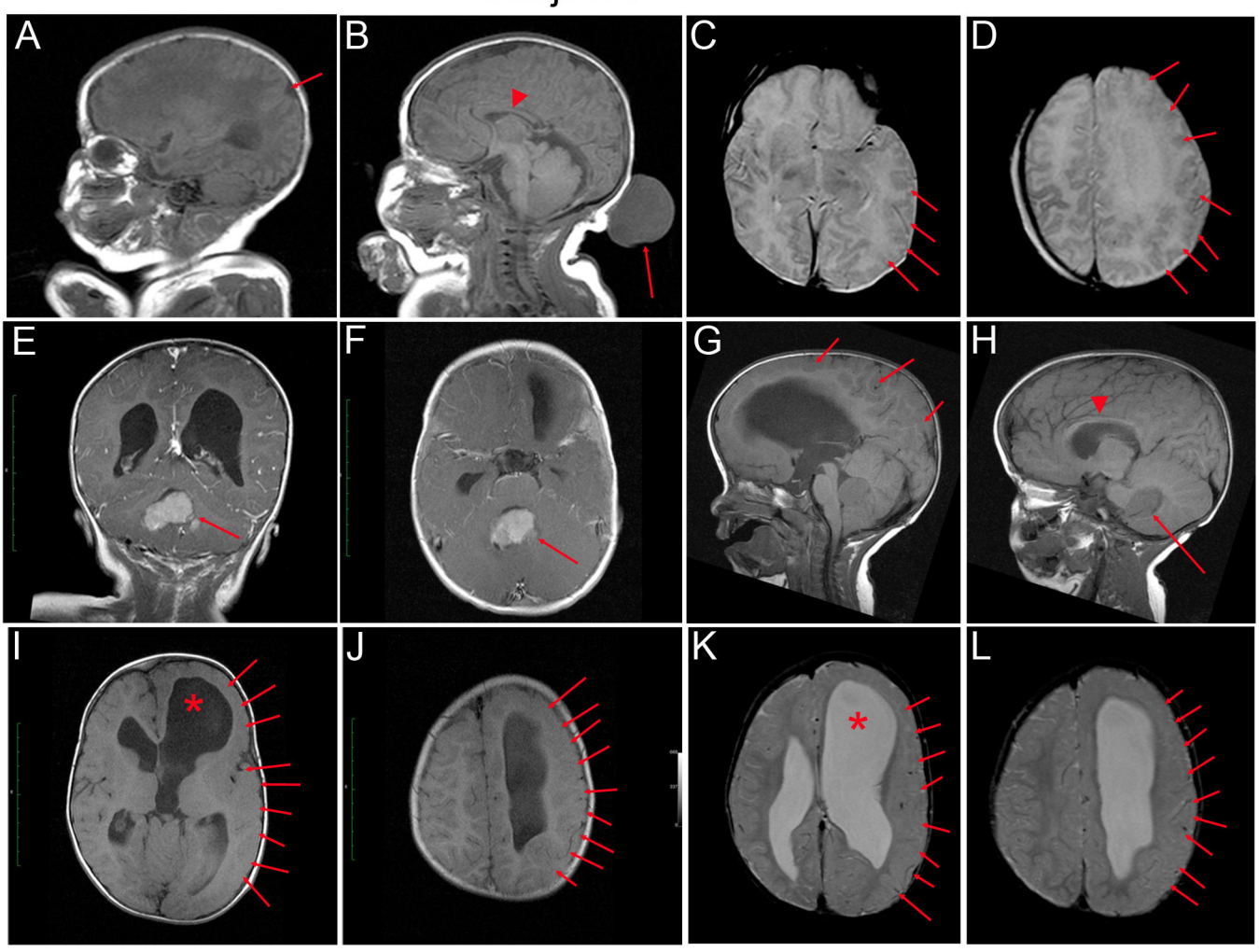

Subject 6

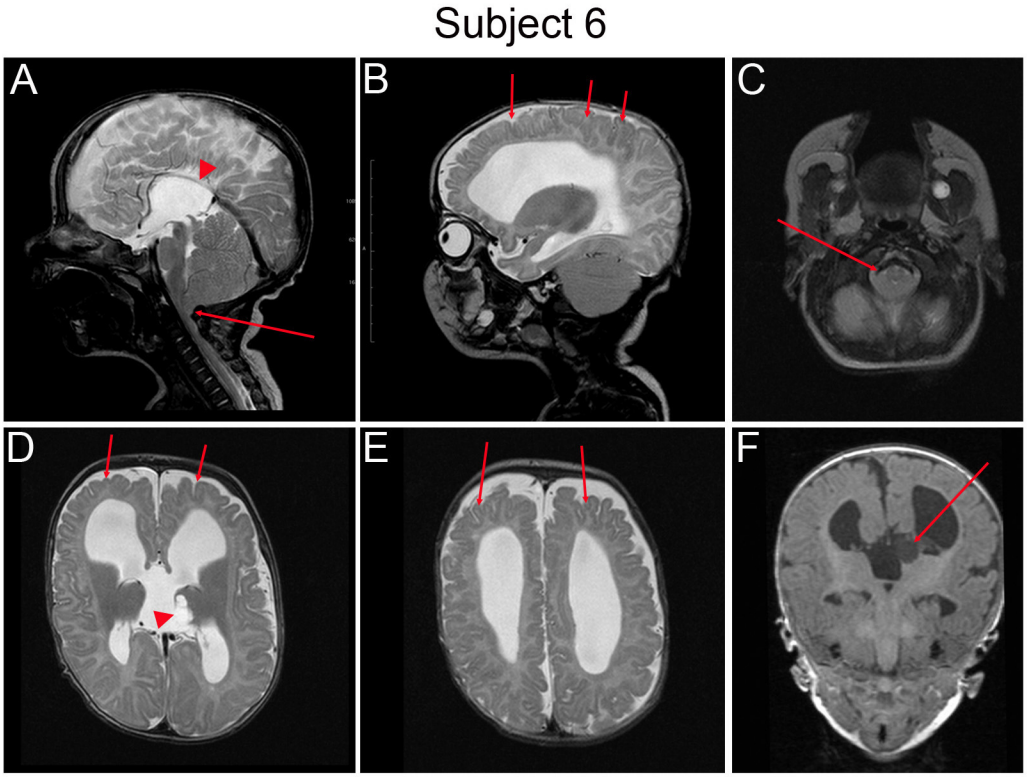

Subject 8

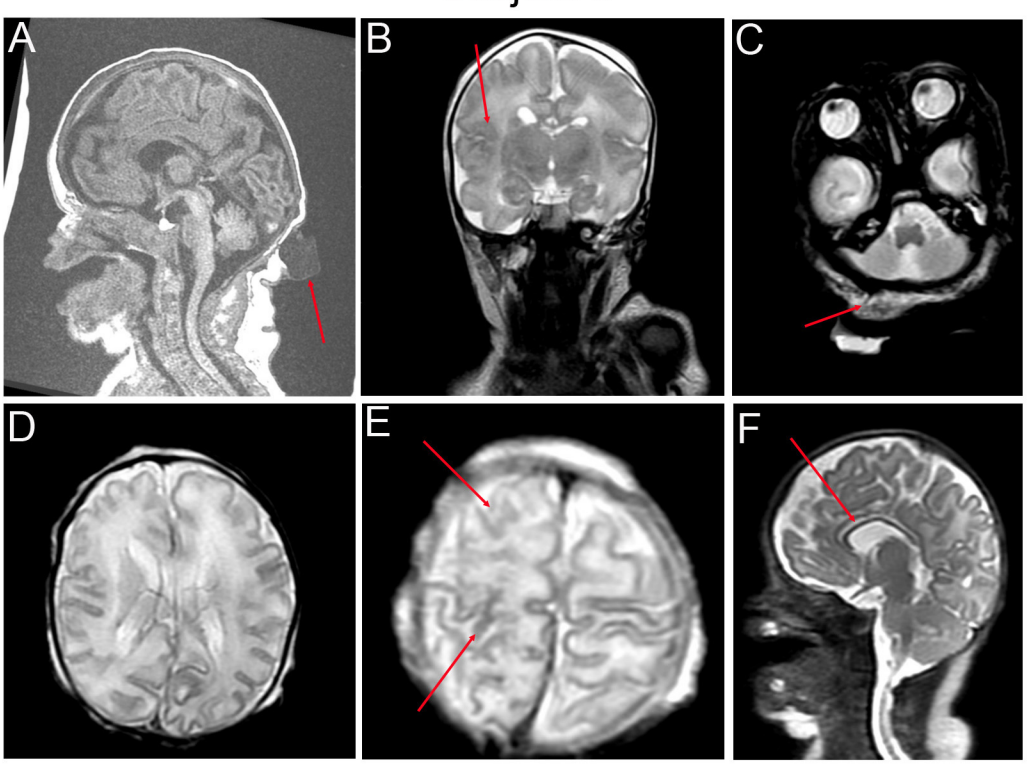

Top, brain MRI from Subject 5 aged 1 day (A-D) and 1 year 5 months (E-L). At 1 day the 4th ventricle is small and pinched with moderate cerebellar ectopia filling the low posterior fossa (B); in the second scan this has evolved to a more severe Chiari I malformation (G). In A and G note macrocephaly with prominent forehead and narrow extra-axial spaces. In B, the corpus callosum is shortened with absent rostrum and splenium consistent with partial agenesis (ACC, arrowhead, see also image H); note also a 3-4 cm occipital encephalocele connecting to the low posterior fossa (arrow, resected in the later set of images). In C,D,I-L note left hemimegalencephaly (HMEG) and ventriculomegaly (asterisks) with dysplastic cortex over part or all of the enlarged hemisphere with irregular gyral pattern and microgyri (arrows, also in A,G), consistent with polymicrogyria or classic HMEG. A single periventricular nodular heterotopia in the anterior-lateral body of the left lateral ventricle was also seen. In E and F, note large 2-3 cm contrast-enhancing tumour in the right cerebellar hemisphere and 4th ventricle (desmoplastic medulloblastoma also visible in H, arrows).

Middle, brain MRI from Subject 6 aged 3 months showing normal head size and extra axial spaces. In A, note very short and thin corpus callosum consistent with partial ACC (arrowhead), normal brainstem and cerebellar structures, but severe cerebellar tonsillar ectopia filling low posterior fossa and associated Chiari 1 malformation (arrow). In B there are small gyri, shallow sulci and subtle pebbling of cortex white matter border consistent with delicate polymicrogyria (arrows). C shows the cerebellar tonsils wrapped around low medulla (arrow). D, subtle abnormalities of gyri and cortex (arrows), cyst in left thalamus (arrowhead) that connects with 3rd ventricle-midline cyst. E, diffuse, small gyri and shallow sulci (most obvious in frontal lobes, arrows), with subtle pebbling of the cortex-white matter border. F, arrow indicates the cyst in the left thalamus.

Bottom, brain MRI from Subject 8 aged 1 day (A-E) and 19 days (F). A, note prominent forehead, turricephaly, hypoplastic cerebellum and occipital cyst (arrow). In B, simplified gyral pattern bilaterally and subtle cortex irregularity (indicated by the arrow in the right perisylvian region). C, base of the brain showing surface tissue thickening at position of lymphangiomatous malformation (arrow). D, mild hemisphere asymmetry (left>right) with too few gyri on both sides and subtle cortex irregularity. E, delicate polymicrogyria on right side only (arrows). F, thin corpus callosum (arrow) consistent with mild ACC, large 1 x 1.5 cm cavum septi pellucidi. The lymphangiomatous malformation has been resected.

Table S1 Genes for which rare coding variants were called in two of the samples analyzed by exome sequencing

Gene	Chr	Position	Reference			Variant			Function	Nucleotide and amino acid change	Sub-ject
				Reads			Reads				
				F	R		F	R			
CREBBP[a]	16	3779774	-	8	1	TCA	5	0	nonframeshift insertion	NM_004380; c.5271_5272insGAT:p.G1757_E1758insD	3
CREBBP	16	3828048	G	43	25	C	37	19	nonsynonymous SNV	NM_004380; c. 2077C>G:p.P693A	4
DNAH17[b]	17	76464741	T	53	25	C	50	24	synonymous SNV	NM_173628; c. 8763A>G:p.T2912=	4
DNAH17	17	76556949	C	1	9	T	1	5	nonsynonymous SNV	NM_173628; c. 1904G>A:p.C635Y	3
CRIPAK[c]	4	1388318	-	14	29	CACAC	9	21	frameshift insertion	artifact	4
CRIPAK	4	1388944	GTGGAGTGTT	3	1	ATGGAGTGCC	5	0	nonframeshift substitution	artifact	2

Note.— Filters: Exome Variant Server and 1000 genomes allele frequency ≤0.0001, no minimum deleterious score (for nonsynonymous substitutions), minimum variant read depth = 4, exclude variants from solved in-house data. We retained variants of all categories that were called in 25-75% of reads. This generated a final list of 1127 variants. The list shown here was generated after further filtering against the Exome Aggregation Consortium dataset (allele frequency ≤0.00001) and the 3 genes with coding variants shared by two cases are shown in the Table above. Platypus did not call *SMO* c.1234C>T in Subjects 2 and 3 owing to their very low frequencies.

[a]excluded because heterozygous loss-of function mutations cause Rubinstein-Taybi syndrome (MIM: 180849).

[b]excluded because one of the variants is synonymous.

[c]excluded because both the sequence changes are artifacts.

Table S2 Deep sequencing of *SMO* c.1234C>T in CJS samples – read depths and percentage mutant allele

Subject	Tissue sample			C allele	T allele	% T allele
	ID		Source[b]			
1*	1-1	2244	blood	3579	3	0.08
	1-2[a]	2245	eyelid	17507	2145	**10.9**
	1-3	6292	skin	3474	0	0
	1-4[a]	6291	fib (1-3)	1013	975	**49.0**
2*	2-1	1280	skin	24106	7827	**24.5**
	2-2	6736	skin	27755	9	0.03
	2-3[a]	3082	fib (2-1)	2650	109	**3.95**
	2-4	6737	fib (2-2)	14626	767	**4.98**
	2-5	6845	bowel[c]	40869	201	0.49
3*	3-1	6942	skin	38264	6040	**13.6**
	3-2[a]	2252	fib	6455	3	0.05
	3-3	6943	fib (3-1)	3940	12	0.30
	3-4	6640	saliva	2510	42	**1.65**
4	4-1[a]	5843	blood	2310	0	0
	4-2	6723	saliva	1850	2	0.11
5*	5-1	6628	blood	17577	6	0.03
	5-2	6629	saliva	39146	3000	**7.12**
	5-3	6702	meningocele[c]	15364	3806	**19.8**
	5-4	6703	medulloblastoma[c]	12745	9600	**43.0**
6*	6-1	6847	skin[c]	6306	952	**13.1**
6*	6-2	6838	saliva	19924	1137	**5.40**
	6-3	6862	abdominal tumor[c]	1711	993	**36.7**
	6-4	6867	abdominal tumor[c]	5295	2862	**35.1**
7*	7-1	7039A	skin	4224	150	**3.43**
	7-2	7039B	fib (7-1)	5181	193	**3.59**
	7-3	7038B	fib (7-5)	7844	2	0.03
	7-4	6802	saliva	5426	6	0.11
	7-5	7038A	bone marrow	4679	47	0.99
8*	8-1	6839	blood	21600	109	0.50
	8-2	6840	colon[c]	19853	1624	**7.56**
	8-3	6841	cecum[c]	20179	2042	**9.19**
	8-4	6843	bone[c]	859	0	0
	8-5	6842	thumb[c]	8233	0	0
9	9-1	6984	blood	13168	12	0.09
	9-2	7314	saliva	58987	24	0.04
10*	10-1	7634	skin	143303	71845	**33.4**
	10-2	7638	fib (10-1)	169197	32719	**16.2**
Control	11-1	6985	blood	5599	2	0.04
	11-2	6986	blood	3028	1	0.03
	11-3	7002	saliva	54728	6	0.01

[*]Mutation positive; Samples quantified as containing >1% of the c.1234T allele are denoted in bold; [a]Sample used in exome sequencing; [b]Tissue source of DNA, sample ID in brackets indicates the skin sample from which fibroblasts were cultured. DNA was extracted from peripheral blood, saliva and a minimum of three 10 µm FFPE sections using Nucleon BACC3, Oragene-DNA (DNA Genotek) and Qiagen DNA FFPE tissue kits, respectively. DNA from all other tissue was obtained by homogenization, followed by overnight proteinase K treatment, phenol-chloroform extraction and DNA precipitation. The starting tissue from which fibroblast (fib) cultures were derived is indicated in brackets. [c]FFPE samples.

Table S3. Primers and amplification conditions used for genetic analysis of *SMO*

Amplification of *SMO* exon 6 for dideoxy sequencing[a]

	Primer sequence 5′→3′		Product size (bp)
Amplicon	Forward	Reverse	
SMO exon 6	caggtggatggggactctgtgagtgg	ttcgtctgcctagagggtcaccttctact	285

Deep sequencing – 1st round amplification of *SMO*[b]

	Primer sequence 5′→3′		Product size (bp), not including tags
Amplicon	Forward (tag lowercase, gene-specific sequence uppercase)	Reverse (tag lowercase, gene-specific sequence uppercase)	
Exon 1-1	cgctcttccgatctctgGCTTTTGCTGAGTTGGCGG	tgctcttccgatctgacCCAGTCACCGCCGCGC	194
Exon 1-2	cgctcttccgatctctgGGCGGGAGCGCGAGGA	tgctcttccgatctgacACCAGAGCACGAGCTTGCCGT	196
Exon 1-3	cgctcttccgatctctgACTCGGACTCCCAGGAGGAAG	tgctcttccgatctgacGCACGTAACCTGCCCCCAAAG	204
Exon 2-1	cgctcttccgatctctgAGGTCTGACCAGTGATGGGCT	tgctcttccgatctgacACCCGGTCATTCTCACACTTG	200
Exon 2-2	cgctcttccgatctctgGATCCAGCCCCTGCTGTGTGC	tgctcttccgatctgacCAACCCAGAGAGCCTGGACC	215
Exon 3-1	cgctcttccgatctctgCGTCCCTGAGCTGCCTTGAC	tgctcttccgatctgacTGTAGCTGTGCATGTCCTGGT	210
Exon 3-2	cgctcttccgatctctgGCCAGAACCCGCTCTTCACAGA	tgctcttccgatctgacATCATGACCCTTCCCTGGGGA	211
Exon 4-1	cgctcttccgatctctgCAGGGAAGGGTCATGATCAGA	tgctcttccgatctgacCAATGCTGCCCACAAAGAAGC	193
Exon 4-2	cgctcttccgatctctgGAATCGCTACCCTGCTGTTATTCTC	tgctcttccgatctgacCACACTTCAGCCTTCCTCCCTG	198
Exon 5-1	cgctcttccgatctctgGAACCTCCAGACCTCAGCAGC	tgctcttccgatctgacCTTTGAAGGAAGTGTGCCAGGC	218
Exon 5-2	cgctcttccgatctctgGGTTTGGTTTGTGGTCCtcacc	tgctcttccgatctgacCCCCTCCCTCAAACTCACCC	208
Exon 6	cgctcttccgatctctgAGTAACCCACCTTCTGTCCCA	tgctcttccgatctgacCCAACTGGTCCTGGCCTGGT	191
Exon 7	cgctcttccgatctctgCTCACCCCTGCTAATGTCTGA	tgctcttccgatctgacGGTCGCATAGCCCCAGGA	206
Exon 8	cgctcttccgatctctgGACTCTCTCCTCCCCACTGCTG	tgctcttccgatctgacCCGCCTCCATGCCCCTCA	203
Exon 9-1	cgctcttccgatctctgTGGGTGACAGAGCAAGATCCT	tgctcttccgatctgacGTTCCAAACATGGCAAACAGGT	203
Exon 9-2	cgctcttccgatctctgGCCTTCTGGTGGAGAAGATCA	tgctcttccgatctgacTAGAGGCAGGACCCGACAAAA	201
Exon 10-1	cgctcttccgatctctgAGAGAAGGCCTCTACTCCTGAGTCC	tgctcttccgatctgacGGCAATCATCTTGCTCTTCTTGATC	206
Exon 10-2	cgctcttccgatctctgGCAGAGTGACGATGAGCCAAAG	tgctcttccgatctgacTGCCCCCAGCAGGCTGG	220
Exon 11	cgctcttccgatctctgGACCGGGAAGTCACTATTCCTTC	tgctcttccgatctgacCCCACCTTCCTCCAGAAGCT	217
Exon 12-1	cgctcttccgatctctgGCATGGACAGAGCCAGGGC	tgctcttccgatctgacGGTACTGGGGGCAGGGGCA	214
Exon 12-2	cgctcttccgatctctgCGCCTGGGCCGGAAGAAG	tgctcttccgatctgacGGGCTCTGGGCAGAATGGG	222
Exon 12-3	cgctcttccgatctctgGGGAGCTGGGGACTCTTGC	tgctcttccgatctgacCTCTTTCCTGTCCCAGGTCCTGC	240

Deep sequencing – 2nd round amplification of *SMO* fragments to incorporate barcodes and Ion Torrent PGM-specific primers[c]

	Primer sequence 5′→3′		Product size (bp)
	Forward (PGM-A sequence uppercase, 10 bp barcode, tag lowercase)	Reverse (PGM-P1 sequence uppercase, tag lowercase)	
Barcoding PCR	CCATCTCATCCCTGCGTGTCTCCGACTCAGxxxxxxxxxxcgctcttccgatctctg	CCTCTCTATGGGCAGTCGGTGATtgctcttccgatctgac	288-337

Note.—[a]DNA amplification was performed in a total volume of 20 µl containing 15 mM TrisHCl (pH 8.0), 50 mM KCl, 2.5 mM $MgCl_2$, 100 µM each dNTP, 0.4 µM primers, and 0.5 units of FastStart polymerase (Roche). Cycling conditions consisted of an 8 min denaturation step at 94°C, followed by 35 cycles of 94°C for 30 s, 68°C for 30 s and 72°C for 30s, with a final extension at 72°C for 10 min.
[b]The entire *SMO* coding region was amplified using tagged primers to generate products of approximately 200 bp (some exons required overlapping amplicons). Reactions used 0.02 U/µl of high fidelity Taq polymerase Q5 (NEB) in a volume of 25 µl containing, 40 ng DNA, 0.5 µM primers, 25 mM Tap-HCl (pH 9.3), 50 mM KCl, 2 mM $MgCl_2$, 1 mM ß-mercaptoethanol and 200 µM each dNTP. Cycling consisted of 30 s of denaturation at 98°C, followed by 15 cycles of 98°C for 10 s, 64°C for 20 s with a 0.5°C decrease each cycle and 72°C for 30s, and then a further 15 cycles of 98°C for 10 s, 57°C for 20 s and 72°C for 30s, with a final extension at 72°C for 2 min.
[c]Amplification products were diluted 1/100 and 2 µl used in a second round PCR, with a common reverse primer including the Ion Torrent PGM P1 adapter, and forward primers with Illumina 10 bp barcodes (to differentiate samples) and the Ion Torrent A adapter sequence. Reactions were set up as above in the first round PCR; cycling consisted of a 30 s denaturation step at 98°C, followed by 9 cycles of 98°C for 10 s, 60°C for 30 s and 72°C for 30s, with a final extension at 72°C for 2 min. Amplification products (roughly equal amounts as judged by EtBr staining in agarose gels) were combined and then purified with AMPure beads (Beckman Coulter). Emulsion PCR and enrichment was performed with the Ion PGM Template OT2 200 Kit (Life Technologies) according to the manufacturer's instructions. Sequencing of enriched templates was carried out on the Ion Torrent PGM (Life Technologies) for 125 cycles using the Ion PGM Sequencing 200 kit v2 and Ion 314 or 316 chips. Data were processed with Ion Torrent platform-specific pipeline software v4.2.1.

Table S4 Deep sequencing of *SMO* in trichoblastoma and nevus sebaceus (NS) samples

		SMO c.1234C>T			Analysis of entire *SMO* coding region			
	Sample	C allele	T allele	% T allele	Av reads all amplicons	Av base coverage	Min read depth	Variants with <1% minor allele frequency
Trichoblastoma	1	5257	2	0.04	2730	2042	217	
	2	3790	7	0.18	2244	1586	136	
	3	3819	20	0.52	1712	1182	83	
	4	3004	3	0.10	1463	1017	75	
	5	3334	6	0.18	1695	1106	142	rs201383344 (5′ end intron 3)
	6	201	1	0.50	998	595.9	48	
	7	3733	2	0.05	1376	982.3	99	
	8	4303	2	0.05	847	621.2	164	
	9	2433	3	0.12	1177	778.7	160	
	10	11237	9	0.08	4275	3098	645	rs201383344
	11	14904	7	0.05	1303	905.8	9	rs193242977; intronic homozygous G>A at 128,843,165 (hg19)
	12	2324	0	0	872	590.4	62	
	13	5206	16	0.31	1341	925.8	156	

	14	4394	3	0.07	1702	1177	177	
NS	1	3200	1	0.03	1653	1159	246	

Table S5 Comparison of brain imaging in Subjects 5, 6 and 8

	Subject 5	Subject 6	Subject 8
Brain malformation			
Occipitofrontal circumference	+3 SD	+4 SD	-0.2 SD
Cerebral asymmetry (or HMEG)	moderate	none	mild
Polymicrogyria (or FCD type 2)	+++	++	+
	L HMEG	PMG in FL	PMG R-PS
Ventriculomegaly (or hydrocephalus)	+	++	n
Agenesis of the corpus callosum	partial	partial	partial
Thalamic cyst	n	y	n
Meningocele	y	n	n
Chiari malformation type 1	y	y	n
Medulloblastoma in cerebellum and 4^{th} ventricle	y	n	n

Note.—abbrevations used: HMEG, hemimegalencephaly; FCD, focal cortical dysplasia; PMG, polymicrogyria; FL, frontal lobe; R-PS, right perisylvian region; y, yes; n, no.